








Effects of a Guide Field on the Larmor Electric Field and Upstream Electron Temperature Anisotropy in Collisionless Asymmetric Magnetic Reconnection

Surapat Ek-In¹ , Kittipat Malakit^{2,1} , David Ruffolo¹ , Michael A. Shay³ , and Paul A. Cassak⁴ 

¹Department of Physics, Faculty of Science, Mahidol University, Bangkok, Thailand

²Department of Physics, Faculty of Science and Technology, Thammasat University, Pathum Thani, Thailand; kmalakit@gmail.com

³Department of Physics and Astronomy, University of Delaware, Newark, DE, USA

⁴Department of Physics and Astronomy, West Virginia University, Morgantown, WV, USA

Received 2017 April 11; revised 2017 June 11; accepted 2017 July 5; published 2017 August 17

Abstract

We perform the first study of the properties of the Larmor electric field (LEF) in collisionless asymmetric magnetic reconnection in the presence of an out-of-plane (guide) magnetic field for different sets of representative upstream parameters at Earth’s dayside magnetopause with an ion temperature greater than the electron temperature (the ion-to-electron temperature ratio fixed at 2) using two-dimensional particle-in-cell simulations. We show that the LEF does persist in the presence of a guide field. We study how the LEF thickness and strength change as a function of guide field and the magnetospheric temperature and reconnecting magnetic field strength. We find that the thickness of the LEF structure decreases, while its magnitude increases when a guide field is added to the reconnecting magnetic field. The added guide field makes the Larmor radius smaller, so the scaling with the magnetospheric ion Larmor radius is similar to that reported for the case without a guide field. Note, however, that the physics causing the LEF is not well understood, so future work in other parameter regimes is needed to fully predict the LEF for arbitrary conditions. We also find that a previously reported upstream electron temperature anisotropy arises in the vicinity of the LEF region both with and without a guide field. We argue that the generation of the anisotropy is linked to the existence of the LEF. The LEF can be used in combination with the electron temperature anisotropy as a signature to effectively identify dayside reconnection sites in observations.

Key words: magnetic reconnection – methods: numerical – plasmas – solar–terrestrial relations

1. Introduction

Magnetic reconnection is an important plasma process that converts the energy stored in magnetic fields into heat and kinetic energy. It plays a crucial role in many magnetized plasma systems, such as governing the dynamics of Earth’s magnetospheric plasma system and rearranging the coronal magnetic field configuration and releasing energy in the form of solar and stellar flares and coronal mass ejections. Reconnection occurs in a diffusion region in which the plasma is no longer ideal. Understanding the physics of the diffusion region of collisionless reconnection, containing both an ion diffusion region and a smaller electron diffusion region, is therefore a key to understanding reconnection as a whole. The physics of the diffusion region, especially the electron diffusion region, is considered sufficiently important that the *Magnetospheric Multiscale (MMS)* mission (Burch et al. 2015) is mainly dedicated to studying it in the Earth’s magnetosphere.

An issue for high-resolution instruments such as those on the *MMS* is that they can produce data at a rate that exceeds the available downlink capacity. Therefore, only promising time intervals are selected for full downlink (Burch & Drake 2009; Burch et al. 2015). To aid the real-time selection process, signatures for the diffusion region and its surroundings are crucial.

Based on a particle-in-cell (PIC) simulation study of anti-parallel asymmetric reconnection, a new in-plane electric field structure called the Larmor electric field (LEF) was identified (Malakit et al. 2013). The LEF is adjacent to the in-plane “Hall electric field” structure dominated by the $\mathbf{J} \times \mathbf{B}/(n_e e c)$ term in the generalized Ohm’s law, where n_e is the electron density, e is the proton charge, \mathbf{J} is the current density and \mathbf{B} is the

magnetic field. Note that in this manuscript, by “Hall electric field,” we mean the very strong sunward-pointing electric field during asymmetric magnetic reconnection at the Earth’s magnetopause (André et al. 2004; Vaivads et al. 2004; Mozer et al. 2008; Tanaka et al. 2008). At the magnetopause, this electric field is located in the area of strong out-of-plane current on the magnetospheric side of the x-line. In contrast, the LEF points away from the X-line, or Earthward, and is farther into the magnetosphere than the Hall electric field. It was proposed that the LEF could possibly be used as a signature for the region immediately upstream on the magnetospheric side of the ion diffusion region of dayside reconnection (Malakit et al. 2013). Its presence at a dayside reconnection site has been reported using *Polar* observations by Koga et al. (2014).

Currently, the mechanism of LEF generation is not completely understood. Malakit et al. (2013) argued that the electric field appears to “hold back” hot magnetospheric ions as they cross the stagnation point. This implies that magnetospheric ions play a role in governing the width and the magnitude of the LEF, which was consistent with the PIC simulations for the parameter range studied. Alternately, Shay et al. (2016) and Phan et al. (2016) recently showed using simulation and observation that the inflowing magnetosheath ions can overshoot the diffusion region and enter the magnetosphere. Their bulk flow through the magnetospheric reconnecting field produces a drift out of the reconnection plane, contributing an electric field to the LEF through the ion convection term. Magnetosheath ions penetrating into the magnetosphere and drifting out of the plane near a reconnection site were recently reported in THEMIS observations (Phan et al. 2016). Thus, there remain open questions about the physical cause of the LEF for arbitrary upstream conditions;

Table 1
Upstream Parameters and Key Results of the Simulations in this Study

| Run | $B_{\text{rec},1}$ | $B_{\text{rec},2}$ | n_1 | n_2 | B_g | $T_{e,1}$ | $T_{i,1}$ | $T_{e,2}$ | $T_{i,2}$ | m_i/m_e | $\delta_{E,\text{Larmor}}$ | E_{Larmor} | $\delta_{e,\text{Anisotropy}}$ |
|-----|--------------------|--------------------|-------|-------|-------|-----------|-----------|-----------|-----------|-----------|----------------------------|---------------------|--------------------------------|
| 1A | 1.0 | 2.0 | 1.0 | 0.1 | 0.0 | 0.67 | 1.33 | 1.67 | 3.33 | 25 | 3.5 | 1.15 | 4.0 |
| 1A* | 1.0 | 2.0 | 1.0 | 0.1 | 0.0 | 0.67 | 1.33 | 1.67 | 3.33 | 100 | 4.0 | 1.15 | 4.0 |
| 1B | 1.0 | 2.0 | 1.0 | 0.1 | 0.5 | 0.67 | 1.33 | 1.67 | 3.33 | 25 | 4.0 | 1.08 | 3.0 |
| 1C | 1.0 | 2.0 | 1.0 | 0.1 | 1.0 | 0.67 | 1.33 | 1.67 | 3.33 | 25 | 3.0 | 1.33 | 3.0 |
| 1D | 1.0 | 2.0 | 1.0 | 0.1 | 2.0 | 0.67 | 1.33 | 1.67 | 3.33 | 25 | 2.0 | 2.33 | 2.0 |
| 2A | 1.0 | 1.5 | 1.0 | 0.1 | 0.0 | 0.67 | 1.33 | 4.59 | 9.16 | 25 | 5.0 | 1.52 | 4.0 |
| 2B | 1.0 | 1.5 | 1.0 | 0.1 | 0.5 | 0.67 | 1.33 | 4.59 | 9.16 | 25 | 5.0 | 1.47 | 4.0 |
| 2C | 1.0 | 1.5 | 1.0 | 0.1 | 1.0 | 0.67 | 1.33 | 4.59 | 9.16 | 25 | 4.5 | 1.92 | 3.0 |
| 2D | 1.0 | 1.5 | 1.0 | 0.1 | 2.0 | 0.67 | 1.33 | 4.59 | 9.16 | 25 | 2.5 | 2.43 | 2.0 |
| 3A | 1.0 | 1.0 | 1.0 | 0.1 | 0.0 | 0.67 | 1.33 | 6.67 | 13.33 | 25 | 8.0 | 1.16 | 7.5 |
| 3B | 1.0 | 1.0 | 1.0 | 0.1 | 0.5 | 0.67 | 1.33 | 6.67 | 13.33 | 25 | 7.5 | 1.39 | 5.0 |
| 3C | 1.0 | 1.0 | 1.0 | 0.1 | 1.0 | 0.67 | 1.33 | 6.67 | 13.33 | 25 | 5.0 | 2.33 | 2.5 |
| 3D | 1.0 | 1.0 | 1.0 | 0.1 | 2.0 | 0.67 | 1.33 | 6.67 | 13.33 | 25 | 3.0 | 3.20 | 1.5 |

both mechanisms can likely be active for various upstream conditions.

Malakit et al. (2013) varied the reconnecting magnetic field strengths, magnetospheric density, and magnetospheric temperature, but treated only anti-parallel reconnection and held the upstream ion-to-electron temperature T_i/T_e fixed at 2, so it only treated a limited region of parameter space. At the dayside magnetopause, reconnection is not always anti-parallel (Paschmann et al. 1986; Scurry et al. 1994; Phan et al. 1996; Burch & Phan 2016; Cassak & Fuselier 2016; Eriksson et al. 2016a, 2016b). Therefore, it is important to understand how the LEF is affected when there is a guide field, i.e., a magnetic field parallel to the X-line and perpendicular to the reconnection plane. Whether the LEF persists and whether it can still be a useful signature when there is a guide field has not yet been determined.

We perform an initial parametric study of the effect of a guide field on reconnection, retaining the assumption that $T_i/T_e = 2$ except where otherwise noted. We show in this study that the LEF structure can still exist in the presence of a guide field. By examining how the width of the LEF varies with upstream parameters, we find that the width of the LEF is linked to the ion Larmor radius. Moreover, the stronger the guide field and smaller the ion Larmor radius, the more localized the LEF structure and the stronger the LEF magnitude. We further find that the electron temperature anisotropy and associated parallel electric field in the upstream region, discussed by Egedal et al. (2011), is present in a similar region as the LEF both with and without a guide field. We argue that this parallel electric field is related to the physics of the LEF, being generated partly by ion pressure gradients and partly by ion inertia terms from magnetosheath ions crossing to the magnetosphere. We conclude that the LEF and electron temperature anisotropy can be used in combination as a stronger signature for dayside reconnection than using the LEF alone.

The simulation setup is discussed in Section 2. Section 3 shows that the LEF exists with a guide field and investigates its scaling on upstream parameters. The coincidence of the LEF and electron temperature anisotropy is discussed in Section 4. Some new insights on the physical mechanism causing the existence of the LEF are discussed in Section 5, including simulations with T_i/T_e different than 2 that underscore the importance of studying the LEF in other parameter regimes. Section 6 has a brief conclusion.

2. Simulation

We use the PIC code P3D (Zeiler et al. 2002) to perform simulations in 2.5 dimensions of collisionless asymmetric reconnection with sets of inflow parameters representing dayside reconnection and with different guide field strengths and magnetosphere-to-magnetosheath reconnecting magnetic field strength ratios. The guide field is modeled as uniform throughout the simulation region.

In the simulations, magnetic field strengths and particle number densities are normalized to arbitrary values B_0 and n_0 , respectively. Lengths are normalized to the ion inertial length $d_{i0} = c/\omega_{pi}$ at the reference density. Time is normalized to the ion cyclotron time $\Omega_{ci0}^{-1} = (eB_0/m_i c)^{-1}$. Speeds are normalized to the Alfvén speed $c_{A0} = B_0/(4\pi m_i n_0)^{1/2}$. Electric fields and temperatures are normalized to $E_0 = c_{A0} B_0/c$ and $T_0 = m_i c_{A0}^2/k_B$, respectively.

Each simulation is performed in a periodic domain of size $L_x \times L_y = 204.8 \times 102.4$. The grid size $\Delta x = \Delta y$ is 0.05. The time step Δt is 0.005. The number of particles per grid cell, ppg , which represents the normalized particle density n_0 , is 200. The ion to electron mass ratio m_i/m_e is 25 except where noted. The speed of light c is 15. The initial conditions represent two current sheets. A small perturbation in the magnetic field is used to initiate the reconnection. Before analyzing the results, the simulations are allowed to evolve until they reach a quasi-steady state, in which the reconnection rate is nearly constant. See Malakit et al. (2010) for more details on the simulation procedures.

We use three sets of upstream parameters in our simulations. For all three sets, the ratio of the density from the two inflow sides n_2/n_1 is 0.1, where the 1 and 2 subscripts denote the magnetosheath and magnetospheric sides, respectively. However, the in-plane upstream magnetic field ratio $B_{\text{rec},2}/B_{\text{rec},1}$ is varied as 1.0, 1.5, or 2.0, with the stronger field on the same side as the lower density. These asymmetries in the density and magnetic field reasonably represent the typical range of dayside magnetospheric reconnection parameters (Phan & Paschmann 1996; Mozer et al. 2008; Tanaka et al. 2008). For each set, the magnitude of the guide field is varied as 0.0, 0.5, 1.0, or 2.0. We fix $T_i/T_e = 2$ on both sides since $T_i > T_e$ for magnetopause applications. The initial upstream parameters on side 1 and 2—magnetic field, density, ion temperature, and electron temperature—and key results are shown in Table 1.

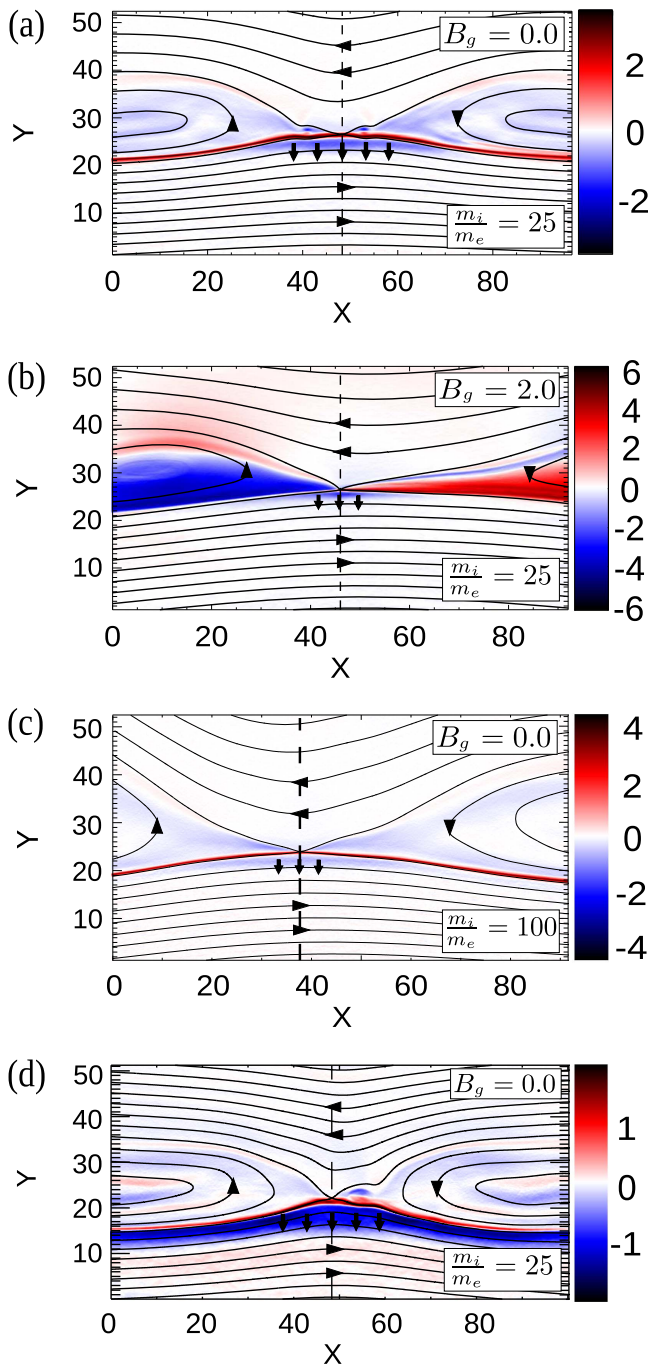


Figure 1. Two-dimensional plots of the electric field in the vertical direction E_y for the cases of (a) zero guide field (Run 1A), (b) non-zero guide field $B_g = 2.0$ (Run 1D), and (c) zero guide field with a different mass ratio $m_i/m_e = 100$ (Run 1A*). Note that (a)–(c) share the same set of upstream parameters ($B_{\text{rec},1} = 1$, $B_{\text{rec},2} = 2$, $n_1 = 1$, $n_2 = 0.1$) that can be considered typical for magnetopause reconnection. (d) is also a case of zero guide field, but with another set of typical magnetopause reconnection parameters ($B_{\text{rec},1} = 1$, $B_{\text{rec},2} = 1$, $n_1 = 1$, $n_2 = 0.1$) (Run 3A). The blue region below the X-line represents the LEF region with arrows pointing downward to indicate the LEF direction. The black lines represent magnetic field lines with arrow heads indicating the magnetic field direction. The dashed line shows a vertical cut through the X-line. (The data for all three different sets of parameter values ($B_{\text{rec},1}$, $B_{\text{rec},2}$, n_1 , n_2) and four different guide field values B_g are provided in the Appendix.)

3. Larmor Electric Field and its Guide Field Dependence

We first demonstrate that the LEF exists in the presence of a guide field. Figures 1(a) and (b) show the in-plane electric field

E_y in Run 1A and 1D, respectively. The only difference between these simulations is that the latter has a guide field of 2, while the former is anti-parallel. For the case with no guide field, the Hall electric field structure is the red region close to the magnetospheric separatrix in panel (a), and the LEF is the blue region with arrows pointing down below the X-line. Panel (b) reveals that there is an analogous downward-pointing in-plane electric field in the guide field case, denoted by the arrows. Therefore, the simulations confirm the LEF structure is still present but more localized in systems with a guide field.

We now determine how properties of the LEF depend on upstream parameters in the presence of a guide field. Two key properties of the LEF are its thickness $\delta_{E,\text{Larmor}}$ and its magnitude E_{Larmor} (Malakit et al. 2013). Consider Figure 2, which shows 1D cuts along the vertical dashed line through the X-lines in Figure 1, to see how the LEF thickness $\delta_{E,\text{Larmor}}$ and the LEF magnitude E_{Larmor} are measured. On the magnetospheric side (left side) of the X-line, there is a bipolar structure of the Hall electric field (positive) and the LEF (negative). The magnitude E_{Larmor} is measured from the peak value of the LEF indicated by the horizontal dashed line. The thickness $\delta_{E,\text{Larmor}}$ is measured as the distance between the two vertical dotted lines. The dotted line on the right, located where E_y switches signs, marks the border between the Hall and the LEF structure. The dotted line on the left, located where E_y becomes zero again, marks the other end of the LEF structure.

We find that the structure of the LEF is modified in the presence of a guide field and that the degree of modification depends on the strength of the guide field. When there is a non-zero guide field, the LEF becomes more localized. We can see that in comparisons between Figure 1(a) for zero guide field and 1(b) for a guide field of 2. The LEF structure (the blue area below the X-line) spans a smaller area compared with its counterpart in Figure 1(a). Thus, we expect the LEF would be more difficult to detect with satellites as the guide field increases. At the same time, the LEF, if observed, ensures closer proximity to the X-line and the ion diffusion region.

While the thickness of the LEF structure becomes smaller when the guide field strength increases, the magnitude of the LEF does the opposite: the stronger the guide field, the larger the magnitude of the LEF. Comparing Figure 2(a), where there is no guide field (Run 1A), to Figure 2(b), where there is a guide field of 2 (Run 1D), one observes the increase in magnitude of E_{Larmor} (the negative peak of E_y) from about 1.2 to 2.3 as well as the decrease in the thickness of the LEF $\delta_{E,\text{Larmor}}$ from about 3.5 to 2.

To study the factors affecting the width and strength of the LEF, in Figure 3 we plot $\delta_{E,\text{Larmor}}$ and E_{Larmor} versus the upstream parameters that are changed in this study: $B_{\text{rec},2}$, B_g , and $T_{e,2}$. Note that although $T_{e,2}$ is varied to maintain pressure balance, the LEF is a kinetic ion effect so there is not expected to be any intrinsic dependence on electron dynamics. We measure the LEF thickness $\delta_{E,\text{Larmor}}$ and the LEF magnitude E_{Larmor} with three sets of upstream parameters representing typical dayside magnetopause reconnection and with four different values of guide field for each set as shown in Table 1. Figure 3 shows these quantities for the new simulation results (the solid symbols) as well as the results from Malakit et al. (2013) (the open symbols), which is a zero guide field study, plotted as a function of the initial upstream parameter of interest. For all four of the varying parameters there is significant spread in the data, but some general behaviors are

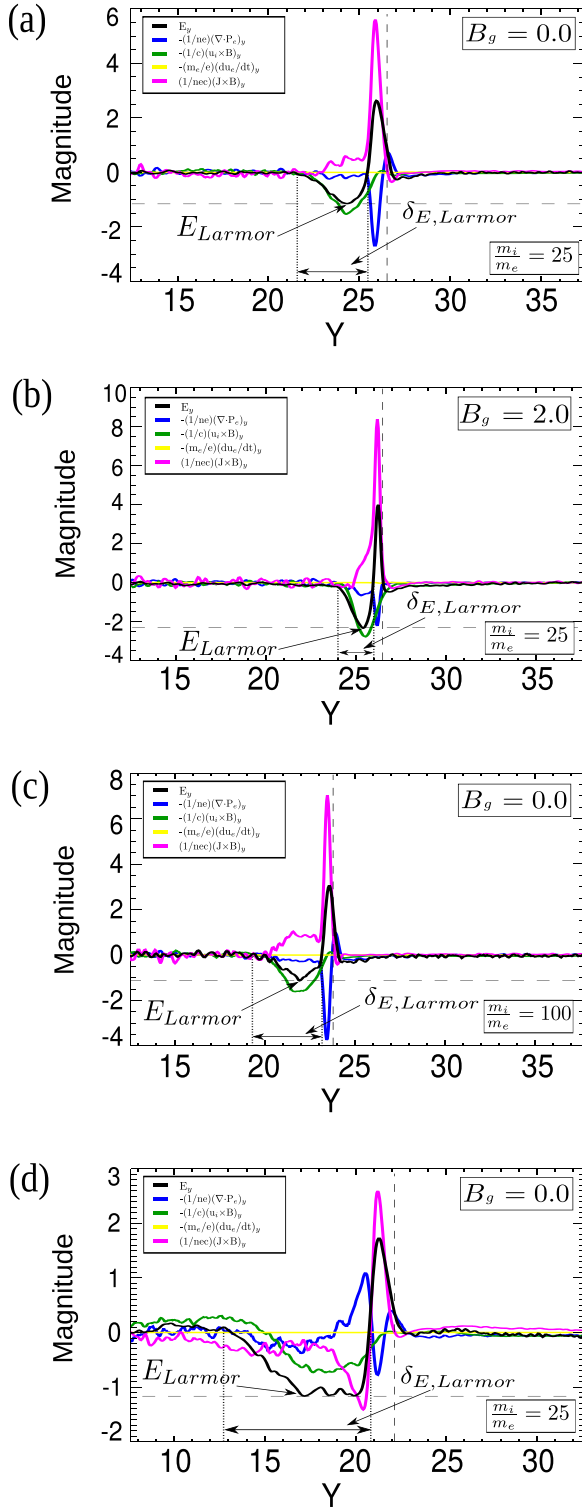


Figure 2. Vertical cut of E_y through the X-line as shown by the dashed line in Figure 1, for the same four simulations. In each plot, the vertical dashed line is provided to show the y position of the X-line for reference. The two vertical dotted lines mark the boundaries of the LEF structure. The distance between the two lines represents the thickness of the LEF structure $\delta_{E,Larmor}$. The horizontal dashed line marks the magnitude of the LEF E_{Larmor} . The contributions from different terms in the generalized Ohm’s law are shown in different colors as indicated in the box on the upper left of each plot. (The data for all three different sets of parameter values ($B_{rec,1}$, $B_{rec,2}$, n_1 , n_2) and four different guide field values B_g are provided in the Appendix.)

evident. First, an increasing guide field (Figures 3(b) and (f)) tends to decrease the width of the LEF while increasing its magnitude; a similar behavior is evident in Figures 3(c) and (g) for the total magnetospheric field. Finally, an increase in magnetospheric ion temperature (Figure 3(e)) tends to increase the width of the LEF.

The particular mechanism or mechanisms generating the LEF are not fully understood as to whether it is there to prevent magnetospheric ions from flooding into the diffusion region due to their finite Larmor radius (Malakit et al. 2013) or whether it is a natural consequence of finite Larmor radius of magnetosheath ions penetrating into the magnetosphere (Phan et al. 2016; Shay et al. 2016). It seems clear, however, that the Larmor radius of ions is playing an important role, which is consistent with the trends shown in Figure 3. Consider the scaling of the ion Larmor radius,

$$\rho_i \sim \frac{c\sqrt{m_i k_B T_i}}{eB}, \quad (1)$$

where k_B is the Boltzmann constant and B is the total magnetic field magnitude,

$$B = \sqrt{B_{rec}^2 + B_g^2}, \quad (2)$$

where B_{rec} is the in-plane reconnecting magnetic field. The introduction of a guide field in addition to the existing in-plane reconnecting magnetic field makes the total magnetic field stronger and consequently makes the ion Larmor radius smaller, while an increase in temperature makes the ion Larmor radius larger.

As both magnetospheric and magnetosheath ions have been implicated in the physics of the LEF, we explore the LEF scaling using both magnetosheath (side 1) and magnetospheric (side 2) ion temperatures. We define $\rho_{i,2}$ as the Larmor radius using asymptotic magnetospheric ion temperature and magnetic field; $\rho_{i,1*}$ is calculated using the asymptotic sheath ion temperature but using the magnetospheric magnetic field. The dependence of $\rho_{i,2}$ and $\rho_{i,1*}$ on $\delta_{E,Larmor}$ are shown in Figures 4(a) and (b), respectively. There is a general trend of increasing $\delta_{E,Larmor}$ for increasing $\rho_{i,2}$ and $\rho_{i,1*}$. While $\delta_{E,Larmor}$ and $\rho_{i,2}$ correlated reasonably well for the simulations performed in the present study, the fit for $\rho_{i,sh*}$ is less clear; there is a striking spread of $\delta_{E,Larmor}$ points for $\rho_{i,1*} \approx 1.15$ for the simulations without a guide field that suggest the two quantities are not linearly related.

Given that the results for $\delta_{E,Larmor}$ with a guide field are consistent with the expression tested in Malakit et al. (2013), we also compare the magnitude of the LEF versus the Malakit et al. (2013) prediction for the magnitude of the LEF given by

$$E_{Larmor} \sim \frac{k_B T_{i,2}}{e\rho_{i,2}}, \quad (3)$$

where $T_{i,2}$ is the magnetospheric asymptotic ion temperature. As before, $\rho_{i,2}$ includes both the asymptotic reconnecting and guide magnetic fields. If this expression remains valid, the introduction of a guide field into the system would result in a larger E_{Larmor} . The results of comparing the measured E_{Larmor} for the simulations in the present study with Equation (3) are shown in Figure 4(c). The two quantities agree quite well. The

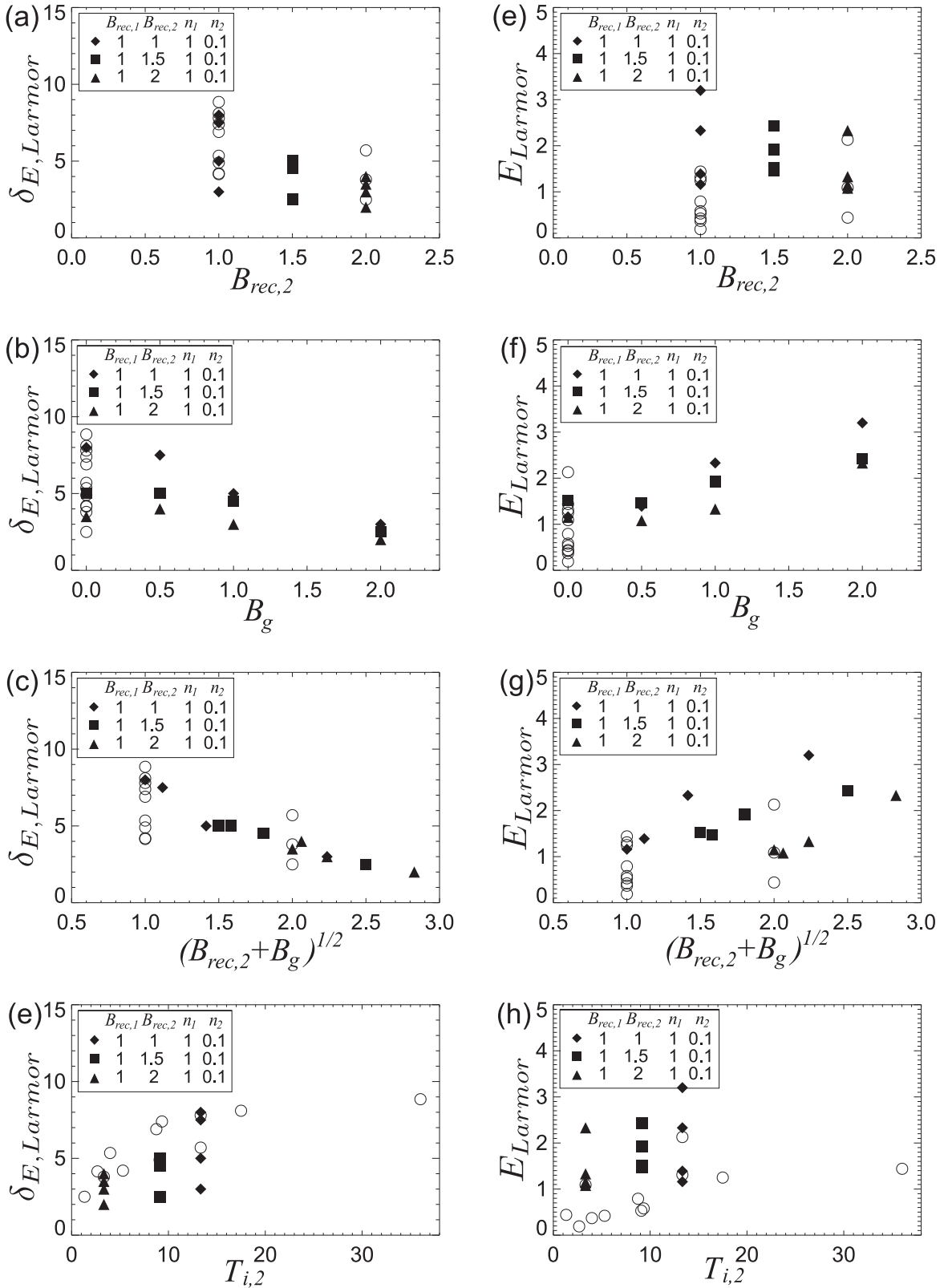


Figure 3. Effect of inflow conditions on the LEF properties: (a)–(d) the thickness of the LEF $\delta_{E, Larmor}$ and (e)–(h) magnitude of the LEF E_{Larmor} . Variation with (a), (e) magnetospheric reconnecting field $B_{rec,2}$; (b), (f) guide field B_g ; (c), (g) total magnetospheric field $\sqrt{B_{rec,2}^2 + B_g^2}$; and (d), (h) magnetospheric ion temperature $T_{i,2}$. Because the introduction of a guide field can lead to secondary island formation (Drake et al. 2006), the data presented here are selected from either the upper or lower X-line that is less affected by secondary islands. The data from runs in this study are shown in solid symbols while the data of runs from the zero-guide-field study (Malakit et al. 2013) are plotted with open circles. The ion temperature and the magnetic field used for calculating the scaling estimates are the asymptotic values on the magnetospheric side.

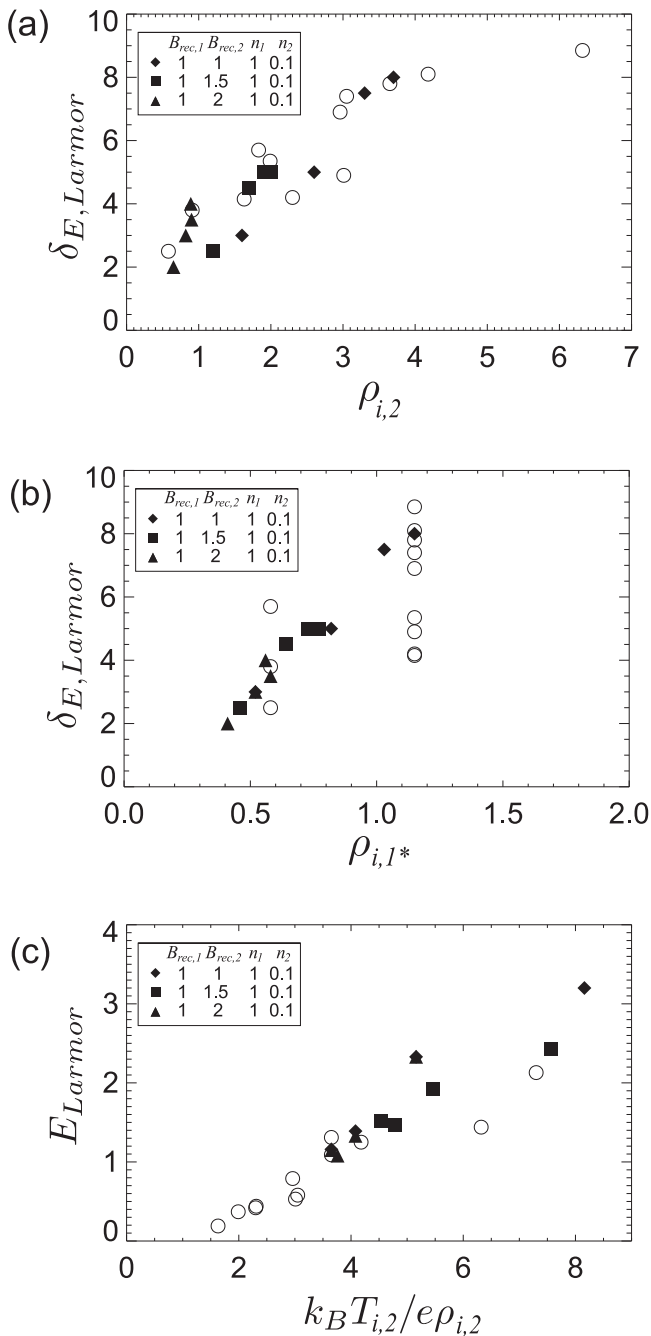


Figure 4. Thickness of the LEF structure $\delta_{E,Larmor}$ vs. (a) asymptotic magnetospheric ion Larmor radius $\rho_{i,2}$ and (b) Larmor radius based on asymptotic magnetosheath ion temperature and magnetospheric total magnetic field $\rho_{i,1*}$. (c) The magnitude of the LEF vs. the Malakit et al. (2013) prediction generalized to include a guide field. The notation is the same as in Figure 3.

comparison shows that for the parameter space explored in this study, Equation (3) from (Malakit et al. 2013) can be generalized to the guide field case.

Apart from affecting the LEF, the introduction of a guide field also affects E_y in the outflow as well. This E_y in the outflow region is caused by the bulk flow in the x -direction and the guide field in the z -direction. With a strong guide field, this newly created E_y can exceed the Hall electric field expected in the case of no guide field as seen on the left of the magnetospheric separatrix in Figure 1(b). With such electric field structures, looking at E_y alone might not be sufficient to

tell whether one is actually in the immediate upstream region of dayside reconnection. However, the following section discusses another structure that can be used in combination with the LEF to help locate the ion diffusion region.

4. Electron Temperature Anisotropy and its Guide Field Dependence

An electron temperature anisotropy also appears in the upstream region on the magnetospheric side of the diffusion region, as identified by Egedal et al. (2011, 2013). This is shown in Figure 5(a) in a plot of the electron temperature anisotropy, defined as $T_{e,\parallel}/T_{e,\perp} - 1$. Red indicates a positive electron temperature parallel anisotropy. This region below the X-line spans a similar (but not exactly the same) area as the blue region below the X-line in Figure 1(a), which is the region of the LEF, as pointed out by Shay et al. (2016). The electron temperature anisotropy requires a parallel electric field (Figures 6(a) and (d)), as identified by Egedal et al. (2011, 2013).

We argue that the physics of ion finite Larmor radius in the LEF region is related to the cause of the parallel electric field. To have the parallel electric field, we need a charge buildup. This can be partially due to the magnetospheric ions that cross the stagnation point and then cause a charge buildup as suggested by the scaling relation for the LEF magnitude Equation (3). In addition, as only magnetosheath ions, not the electrons, can overshoot into the LEF region on the magnetospheric side, these can contribute to a positive charge in the overshoot region. In strongly asymmetric systems, such as those that are typical of the dayside magnetopause, the magnetosheath is significantly more dense than the magnetosphere. It is therefore more likely that the magnetosheath ions are responsible for creating a charge imbalance. This charge imbalance then produces the parallel electric field that pulls magnetospheric electrons into the LEF region to help achieve charge neutrality (Shay et al. 2016). At the same time, this same electric field accelerates the ions toward the downstream region (Figure 6(d)), resulting in the flow of ions parallel to the field toward the outflow directions in the LEF region before the ions cross the separatrix (Figure 6(b)). Such ion outflow overshoot has been observed by spacecraft (Phan et al. 2016). Besides causing a charge imbalance, when the magnetosheath ions overshoot into the region, they change the ion temperature in the region as well (Figure 6(c)). Following a thread of field line as indicated by the curved dashed line in Figure 6(c), we can see that a part of the field line is immersed with varying degree in the region of modified ion temperature. The field line is most immersed at the center and less immersed to the left and right. This leads to a non-zero ion pressure gradient parallel to the magnetic field (Figure 6(d)) and, consequently, partially contributes to the parallel electric field in the LEF region. The combination of the parallel ion acceleration and the parallel ion pressure gradient results in the total parallel electric field (Figure 6(d)) that causes counter-streaming motion of the electrons and the enhanced electron parallel temperature.

Because the generation of the electron temperature anisotropy structure is linked to the LEF structure, which is insensitive to the electron mass, the location of the electron temperature anisotropy structure is insensitive to the electron mass as well. This is confirmed by comparing Figures 5(a) and 7(a), which display the anisotropy for the case of $m_i/m_e = 25$, with Figures 5(c) and 7(c), which display the anisotropy for the

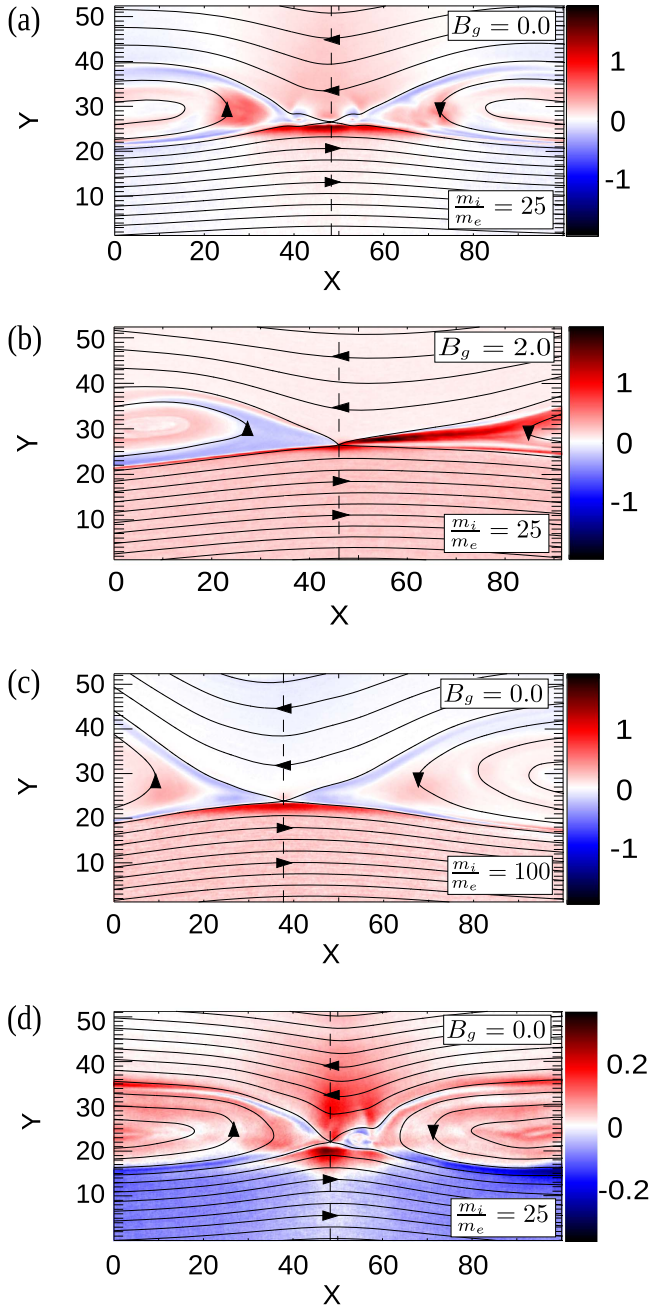


Figure 5. Two-dimensional plot of electron temperature anisotropy $T_{e,\parallel}/T_{e,\perp} - 1$ for the same four simulations shown in Figure 1. The red region below the X-line is the region of high $T_{e,\parallel}$, which is similar to the region where the LEF is present (Figure 1(a)). We note that there is also anisotropy that occurs weakly and uniformly in the upstream regions. This is very likely not physical, but rather numerical. (The data for all three different sets of parameter values ($B_{\text{rec},1}$, $B_{\text{rec},2}$, n_1 , n_2) and four different guide field values B_g are provided in the Appendix.)

case of $m_i/m_e = 100$. There are no significant changes with its overlaps with the LEF structure.

We now compare the thickness of the electron temperature anisotropy structure $\delta_{e,\text{aniso}}$ with the thickness of the LEF structure. We measure $\delta_{e,\text{aniso}}$ as shown in Figure 7. Figure 8 shows that these two physical structures have similar thicknesses for various sets of upstream parameters. We also point out that this continues to be the case when there is a guide field.

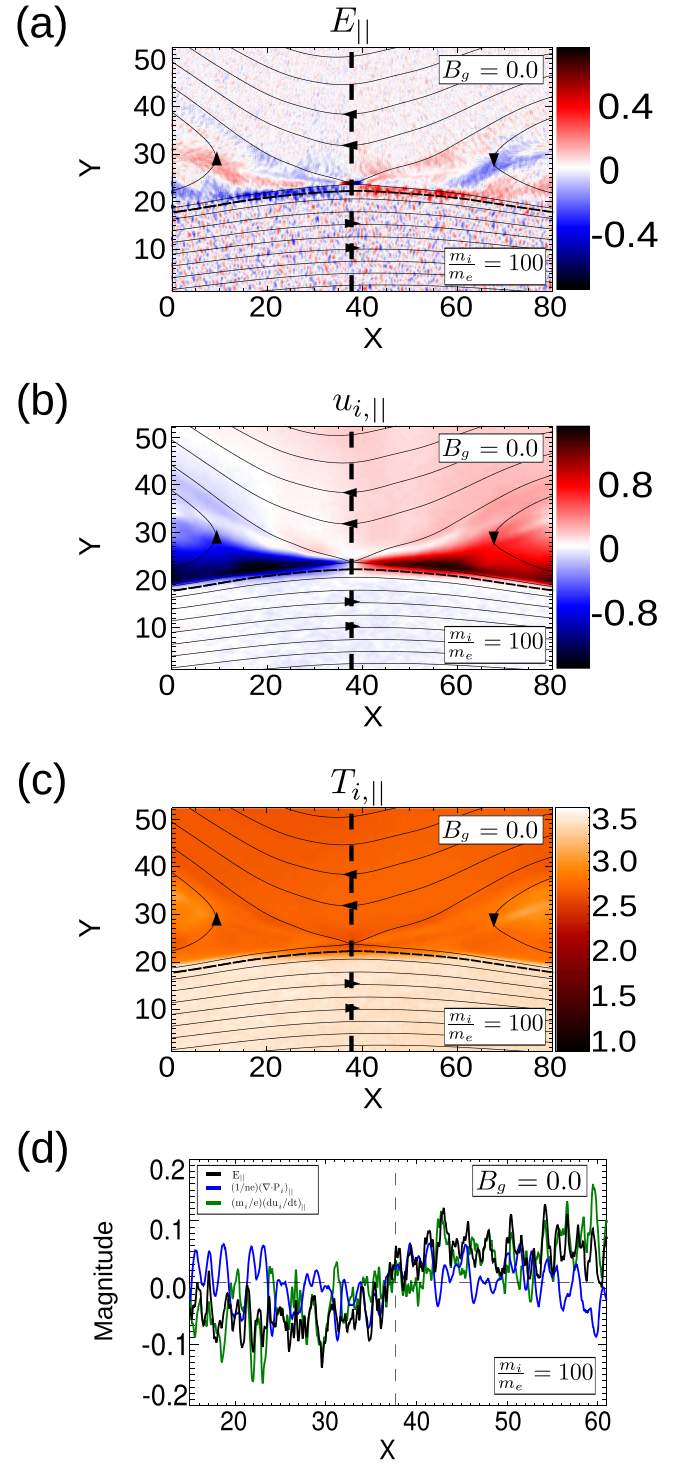


Figure 6. (a) Two-dimensional plot of parallel electric field E_{\parallel} for the cases of zero guide field with a mass ratio $m_i/m_e = 100$ and the upstream parameters ($B_{\text{rec},1} = 1$, $B_{\text{rec},2} = 2$, $n_1 = 1$, $n_2 = 0.1$) that can be considered characteristic of magnetopause reconnection (Run 1A*). (b) 2D plot of parallel ion flow $u_{i,\parallel}$ (c) 2D plot of parallel ion temperature $T_{i,\parallel}$ (d) 1D cuts of E_{\parallel} (black), $(m_i/e)(du_{i,\parallel}/dt)$ (blue), and $(1/ne)(\nabla \cdot P_{\parallel})$ (green) along the magnetic field line indicated by the curved dashed line in (a). The vertical dashed line is provided to show the x position of the X-line for reference. The arrows in (a), (b), and (c) indicate the direction of the magnetic field.

Using both the LEF and the electron temperature anisotropy in combination as a signature for reconnection is more effective than using the LEF or the anisotropy alone. The LEF structure

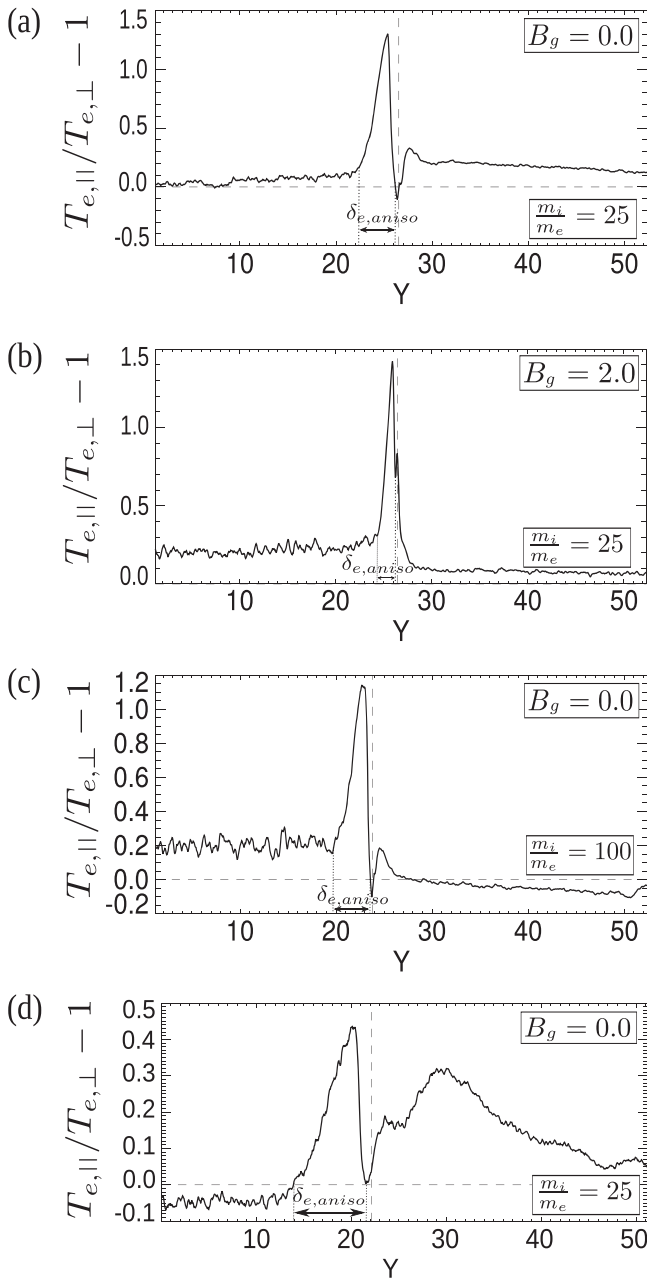


Figure 7. Vertical 1D cut of electron temperature anisotropy $T_{e,||}/T_{e,\perp} - 1$ through the X-line along the dashed lines in Figure 5. The vertical dashed line is provided to show the y position of the X-line for reference. The two vertical dotted lines mark the boundaries of the electron temperature anisotropy region, and the distance between them represents the thickness of the electron temperature anisotropy structure $\delta_{e,aniso}$. (The data for all three different sets of parameter values ($B_{rec,1}$, $B_{rec,2}$, n_1 , n_2) and four different guide field values B_g are provided in the [Appendix](#).)

can sometimes extend far away from the reconnection area (Figure 1(d)). However, the electron temperature anisotropy, with a similar thickness to the LEF's, does not extend to the sides as far, being more confined to the immediate upstream region (Figure 5(d)). Furthermore, as discussed at the end of Section 3, in the case of a strong guide field, the generation of E_y in the downstream region and the suppression of the Hall electric field structure might lead to a misinterpretation of where a satellite locates a diffusion region if we only look for the LEF (Figure 1(b)). Looking at the anisotropy in conjunction with the LEF, the confusion can be eliminated. Figure 5(b)

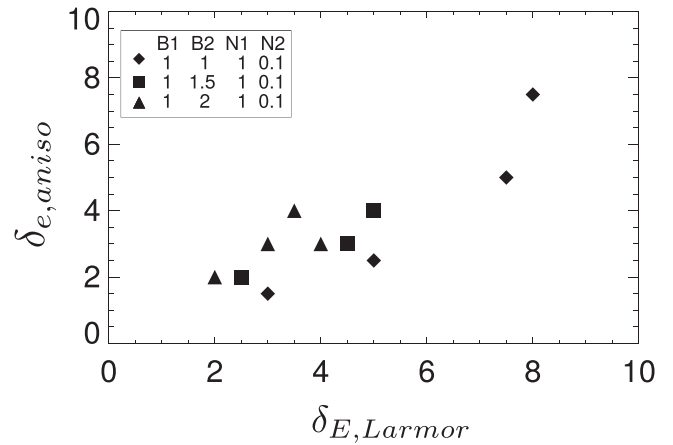


Figure 8. Thickness of the electron temperature anisotropy region $\delta_{e,aniso}$ vs. the thickness of the LEF region $\delta_{E,Larmor}$ for various simulations with and without a guide field. Because an introduction of a guide field into the system can lead to secondary island formation, the data presented here are selected from either the upper or lower X-line that is not or less affected by secondary islands. The direct relationship under a variety of conditions indicates that the electron temperature anisotropy and the LEF are physically related and can be used jointly as a stronger marker of proximity of the diffusion region.

shows that in the vicinity of the magnetospheric separatrix left of the X-line, the anisotropy sharply switches signs making the downstream clear, eliminating the ambiguity caused by looking at E_y alone. Using the anisotropy alone might cause the same boundary problem on the right of the X-line. The E_y signature has a sharp boundary between the immediate upstream and the immediate downstream regions.

5. Discussion on the Larmor Electric Field Mechanism

We emphasize that a general understanding of the mechanism of LEF generation remains elusive. Malakit et al. (2013) argued that magnetospheric ions govern the width and the magnitude of the LEF. However, that model does not capture the involvement of the magnetosheath ions in the generation of the LEF. Shay et al. (2016) and Phan et al. (2016) argued that magnetosheath ions overshoot into the LEF region in the magnetosphere, drift out of plane, and produce a convective electric field that contributes to the LEF. The ion convection term does dominate the LEF in some of the simulations of the present study (such as Run 1A, Run 1D, and Run 1A*; see Figures 2(a)–(c), respectively). However, in the simulation where reconnection is asymmetric only in density (Run 3A), the ion convection term, the Hall term, and the electron pressure gradient term all significantly contribute (Figure 2(d)). This is consistent with the results in Phan et al. (2016), which show that the LEF region is broader than the region where the ion overshoot occurs, suggesting that the ion overshoot is not the sole contributor to the LEF. Furthermore, the penetration of magnetosheath ions into the magnetosphere alone is not adequate to explain the results in Malakit et al. (2013), in which the LEF properties depend on magnetospheric plasma parameters while the magnetosheath plasma parameters are kept unchanged. Therefore, the origin of the LEF likely involves more than one mechanism and depends strongly on the upstream parameters.

We further note that all of the simulations presented thus far in this study and in Malakit et al. (2013) have been performed with $T_i/T_e = 2$ since $T_i > T_e$ is typical at Earth's dayside

$$B_1 = 1.0 \quad B_2 = 1.0 \quad n_1 = 1.0 \quad n_2 = 0.1 \quad B_1 = 1.0 \quad B_2 = 1.5 \quad n_1 = 1.0 \quad n_2 = 0.1 \quad B_1 = 1.0 \quad B_2 = 2.0 \quad n_1 = 1.0 \quad n_2 = 0.1$$

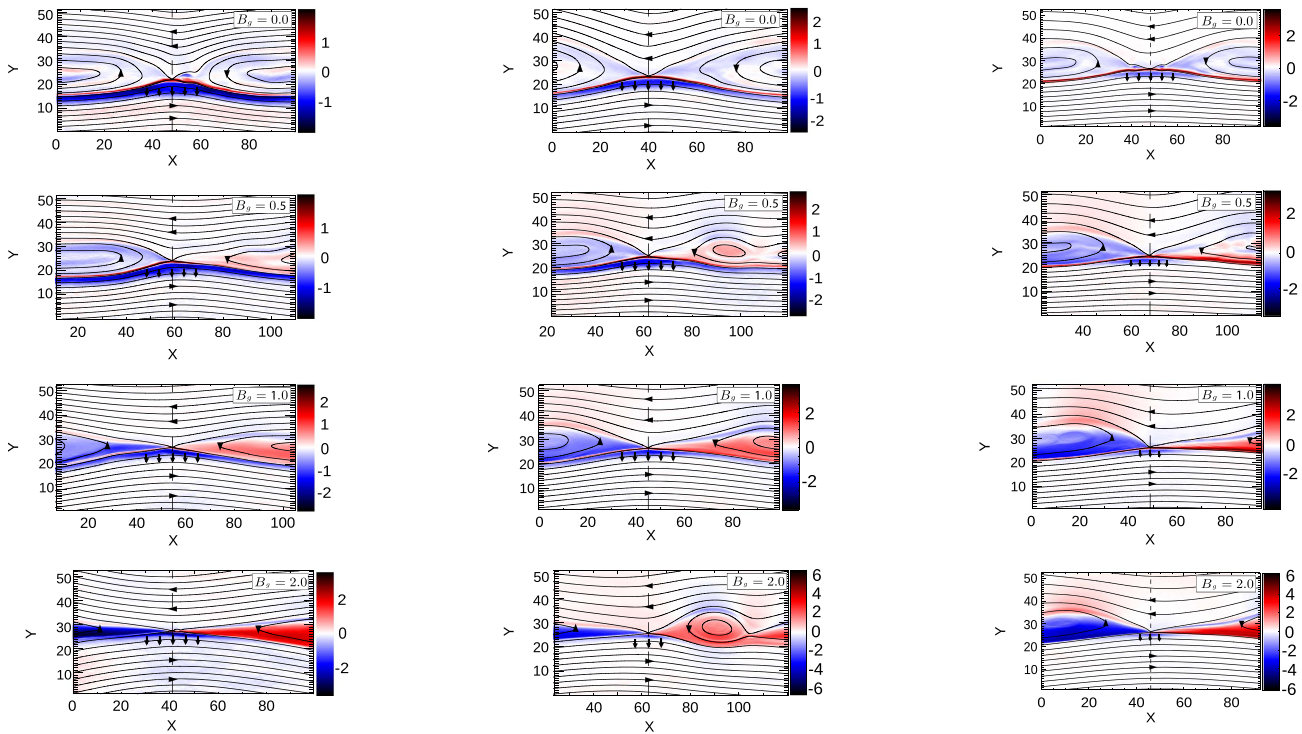


Figure 9. Similar to Figure 1 in the main article. Two-dimensional plots of the electric field in the vertical direction E_y . The blue region below the X-line represents the LEF with arrows pointing downward to indicate the LEF direction. The black lines represent magnetic field lines with arrow heads indicating the magnetic field direction. The dashed line shows a vertical cut through the X-line.

magnetopause. Therefore, key insights of the physics of the LEF will likely be obtained by going beyond this restricted parameter regime. Interestingly, we have preliminary simulation results in the case of $T_i/T_e < 1$ showing that and the scaling relations proposed by Malakit et al. (2013) do not apply in this limit. Thus, future work is needed to determine the roles of the magnetosheath and magnetospheric ions for general asymmetric upstream conditions. Nevertheless, for cases where $T_i > T_e$ such as the dayside magnetopause, the scaling relations are expected to be applicable.

6. Conclusion

We explored the effects of a guide field on the LEF in collisionless asymmetric reconnection using fully kinetic PIC simulations. We demonstrated that the LEF persists in guide field asymmetric reconnection. We analyzed how the LEF varies with changing inflow conditions and have shown that its width and magnitude are strongly linked to the ion Larmor radius; the stronger the guide field, the smaller the Larmor radius, thus the more localized and stronger the LEF. While there are uncertainties regarding the causal agent or agents of the LEF, for the simulation parameter space explored here the scaling estimates of the width and magnitude of the LEF from Malakit et al. (2013) can be generalized successfully for the guide field case. The only modification necessary is that the Larmor radius is determined using the total magnetic field (reconnection and guide).

We also found that in the LEF region, there exists an electron temperature anisotropy, both with and without a guide field.

The electron anisotropy is caused by the parallel electric field, which we argue is generated by both an ion pressure gradient and an inertial ion acceleration due to magnetosheath ions crossing the diffusion region into the magnetospheric side; this leads to a rough co-location of the LEF and the electron temperature anisotropy. Using the electron temperature anisotropy and the LEF together as a signature increases the potential of locating the magnetospheric surrounding of the ion diffusion region for dayside reconnection, which can be useful for *MMS* and other satellites.

We thank T. D. Phan and M. Fujimoto for helpful discussions regarding the physics of the Larmor electric field. This research was supported by the Sri Trung Thong scholarship (S.E.) and postdoctoral research sponsorship (K.M.) of Mahidol University, NSF grants AGS-1219382 (MAS) and AGS-0953463 (PAC), NASA grants NNX08A083G—*MMS* IDS, NNX13AD72G (MAS), NNX16AF75G, and NNX16AG76G (PAC), and Thailand Research Fund grant BRG 5880009 (D.R.) and RTA 5980003 (D.R. and K.M.). Simulations were performed at the National Center for Atmospheric Research Computational and Information System Laboratory (NCAR-CISL). The data used in this study are available upon request to the corresponding author.

Appendix

This Appendix provides provides 4 figures similar to Figures 1, 2, 5, and 7 in the main article, but now including plots for all the different upstream densities, in-plane magnetic field strengths, and guide field values used in our simulations.

$$B_1 = 1.0 \quad B_2 = 1.0 \quad n_1 = 1.0 \quad n_2 = 0.1$$

$$B_1 = 1.0 \quad B_2 = 1.5 \quad n_1 = 1.0 \quad n_2 = 0.1$$

$$B_1 = 1.0 \quad B_2 = 2.0 \quad n_1 = 1.0 \quad n_2 = 0.1$$

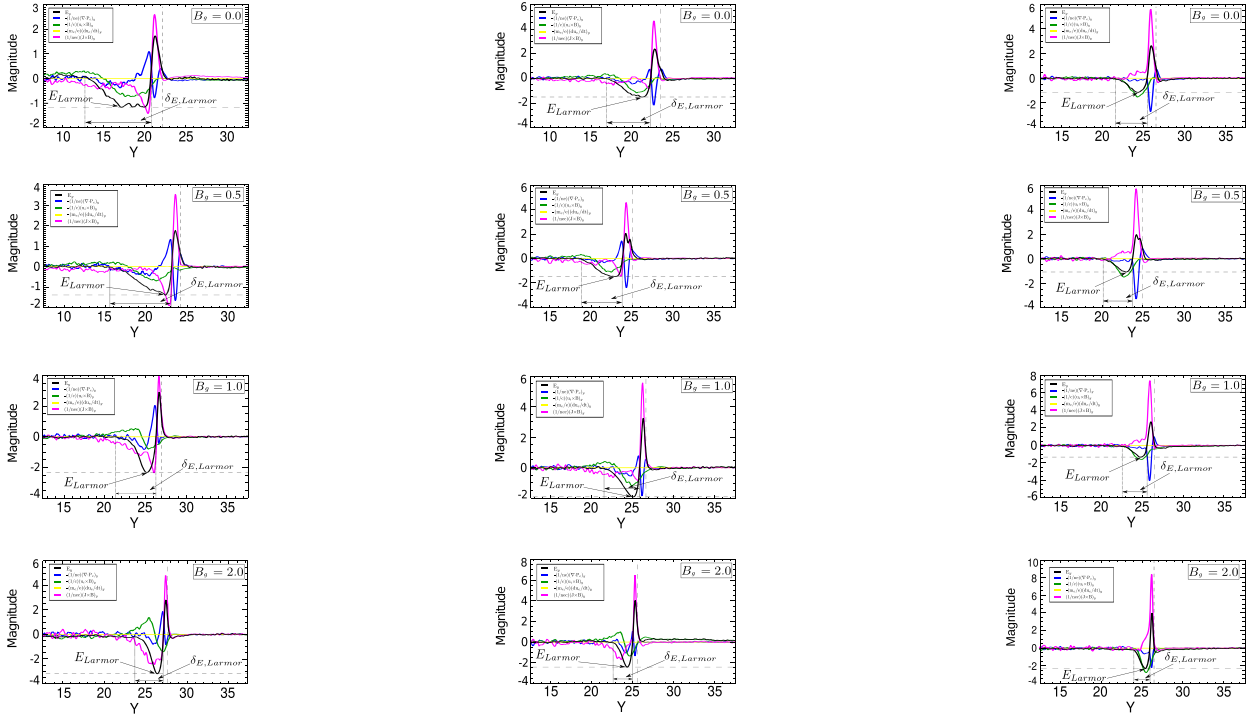


Figure 10. Similar to Figure 2 in the main article. Vertical cut of E_y through the X-line as shown by the dashed line in Figure 1. In each plot, the vertical dashed line is provided to show the y position of the X-line for reference. The two vertical dotted lines mark the boundaries of the LEF structure. The distance between the two lines represents the thickness of the LEF structure $\delta_{E, \text{Larmor}}$. The horizontal dashed line marks the magnitude of the LEF E_{Larmor} . The contributions from different terms in the generalized Ohm's law are shown in different colors as indicated in the box on the upper left of each plot.

$$B_1 = 1.0 \quad B_2 = 1.0 \quad n_1 = 1.0 \quad n_2 = 0.1$$

$$B_1 = 1.0 \quad B_2 = 1.5 \quad n_1 = 1.0 \quad n_2 = 0.1$$

$$B_1 = 1.0 \quad B_2 = 2.0 \quad n_1 = 1.0 \quad n_2 = 0.1$$

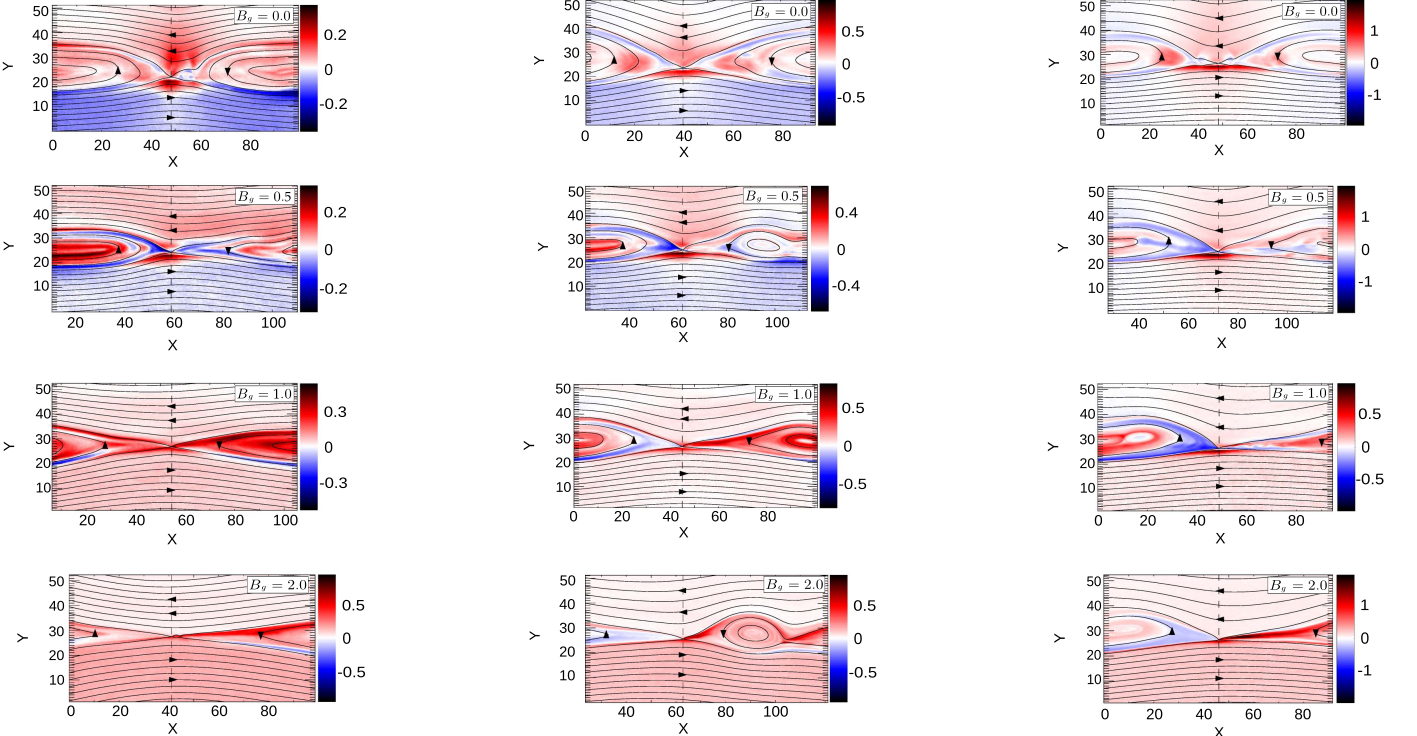


Figure 11. Similar to Figure 5 in the main article. Two-dimensional plot of electron temperature anisotropy $T_{e,||}/T_{e,\perp} - 1$. The red region below the X-line is the region of high $T_{e,||}$, which is similar to the region where the LEF is present (the blue region below the X-line in Figure 1). The black lines represent magnetic field lines with arrow heads indicating the magnetic field direction. The dashed line shows a vertical cut through the X-line.

$$B_1 = 1.0 \quad B_2 = 1.0 \quad n_1 = 1.0 \quad n_2 = 0.1 \quad B_1 = 1.0 \quad B_2 = 1.5 \quad n_1 = 1.0 \quad n_2 = 0.1 \quad B_1 = 1.0 \quad B_2 = 2.0 \quad n_1 = 1.0 \quad n_2 = 0.1$$

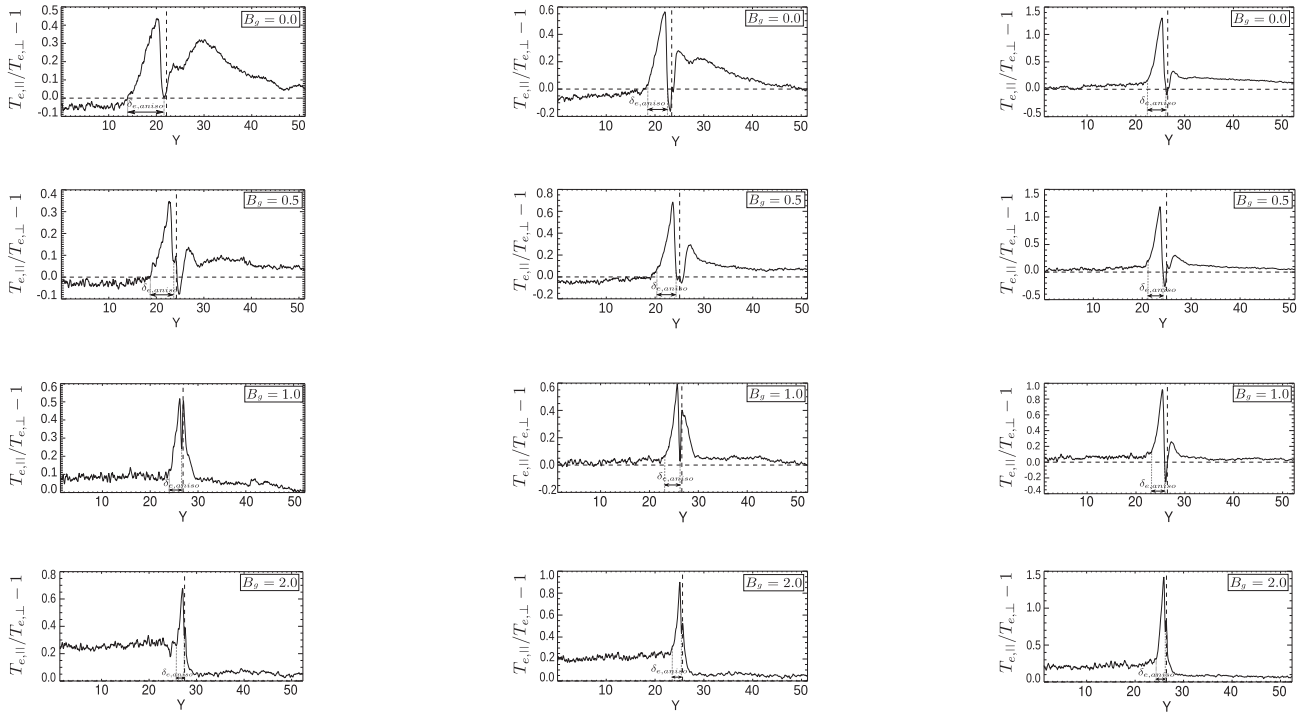


Figure 12. Similar to Figure 7 in the main article. Vertical 1D cut of electron temperature anisotropy through the X-line along the dashed line in Figure 3. In each plot, the vertical dashed line is provided to show the y position of the X-line for reference. The two vertical dotted lines mark the boundaries of the electron temperature anisotropy region, and the distance between them represents the thickness of the electron temperature anisotropy structure $\delta_{e,\text{aniso}}$.

All of our asymmetric reconnection simulations have been performed using the P3D code, a fully kinetic PIC code. The boundaries are periodic in all directions. The initial condition is a double asymmetric current sheet with a small magnetic perturbation to initiate reconnection. Each simulation is allowed to evolve until the reconnection has reached a steady state. Since there is a guide field in our simulations, current sheets are prone to secondary island formation (Drake et al. 2006). We therefore select one X-line from either the upper or lower X-line that is less affected by secondary islands to analyze. Plots of the normal electric field E_y and the electron temperature anisotropy of the selected X-line from all of our simulations are reported in Figures 9–12.

In each figure, the plots are divided into three columns. At the top of each column, there is information about the in-plane magnetic field strengths (B) and number densities (n) of plasma from side “1” (plasma above the X-line in Figures 1 and 3; plasma on the right of the X-line in Figures 2 and 4) and side “2” (plasma below the X-line in Figures 1 and 3; plasma on the left of the X-line in Figures 2 and 4). For each set of B_1 , B_2 , n_1 , n_2 , the guide field B_g is varied from 0.0, 0.5, 1.0, and 2.0 as indicated in the box on the upper right of each plot.

In Figures 11 and 12, where the electron temperature anisotropy is shown, we note that there is also anisotropy that occurs weakly and uniformly in the upstream regions. This is very likely not physical but rather numerical.

ORCID iDs

Surapat Ek-In <https://orcid.org/0000-0002-2232-6760>
Kittipat Malakit <https://orcid.org/0000-0002-0915-5979>

David Ruffolo <https://orcid.org/0000-0003-3414-9666>
Michael A. Shay <https://orcid.org/0000-0003-1861-4767>
Paul A. Cassak <https://orcid.org/0000-0002-5938-1050>

References

- André, M., Vaivads, A., Buchert, S. C., Fazakerley, A. N., & Lahiff, A. 2004, *GeoRL*, **31**, L03803
- Burch, J. L., & Drake, J. F. 2009, *AmSci*, **97**, 392
- Burch, J. L., Moore, T. E., Torbert, R. B., & Giles, B. L. 2015, *SSRv*, **199**, 5
- Burch, J. L., & Phan, T. D. 2016, *GeoRL*, **43**, 8327
- Cassak, P. A., & Fuselier, S. A. 2016, in *Magnetic Reconnection: Concepts and Applications*, ed. W. D. Gonzalez & E. N. Parker (Berlin: Springer), 213
- Drake, J. F., Swisdak, M., Schoeffler, K. M., Rogers, B. N., & Kobayashi, S. 2006, *GeoRL*, **33**, L13105
- Egedal, J., Le, A., & Daughton, W. 2013, *PhPI*, **20**, 061201
- Egedal, J., Le, A., Pritchett, P. L., & Daughton, W. 2011, *PhPI*, **18**, 102901
- Eriksson, S., Lavraud, B., Wilder, F. D., et al. 2016a, *GeoRL*, **43**, 5606
- Eriksson, S., Wilder, F. D., Ergun, R. E., et al. 2016b, *PhRvL*, **117**, 015001
- Koga, D., Gonzalez, W. D., Mozer, F. S., Silveira, M. V. D., & Cardoso, F. R. 2014, *PhPI*, **21**, 100701
- Malakit, K., Shay, M. A., Cassak, P. A., & Bard, C. 2010, *JGR*, **115**, A10223
- Malakit, K., Shay, M. A., Cassak, P. A., & Ruffolo, D. J. 2013, *PhRvL*, **111**, 135001
- Mozer, F. S., Pritchett, P. L., Bonnell, J., Sundkvist, D., & Chang, M. T. 2008, *JGRA*, **113**, A00C03
- Paschmann, G., Baumjohann, W., Sckopke, N., Papamastorakis, I., & Carlson, C. W. 1986, *JGR*, **91**, 11099
- Phan, T. D., & Paschmann, G. 1996, *JGR*, **101**, 7801
- Phan, T.-D., Paschmann, G., & Sonnerup, B. U. Ö 1996, *JGR*, **101**, 7817
- Phan, T. D., Shay, M. A., Haggerty, C. C., et al. 2016, *GeoRL*, **43**, 8844
- Scurry, L., Russell, C. T., & Gosling, J. T. 1994, *JGR*, **99**, 14815
- Shay, M. A., Phan, T. D., Haggerty, C. C., et al. 2016, *GeoRL*, **43**, 4145
- Tanaka, K. G., Retinò, A., Asano, Y., et al. 2008, *AnGeo*, **26**, 2471
- Vaivads, A., Khotyaintsev, Y., André, M., et al. 2004, *PhRvL*, **93**, 105001
- Zeiler, A., Biskamp, D., Drake, J. F., et al. 2002, *JGRA*, **107**, 1230